BIOCHEMISTRY
including biophysical chemistry & molecular biology

Article

pubs.acs.org/biochemistry

Mössbauer and EPR Study of Iron in Vacuoles from Fermenting *Saccharomyces cerevisiae*

Allison L. Cockrell,[†] Gregory P. Holmes-Hampton,[‡] Sean P. McCormick,[‡] Mrinmoy Chakrabarti,[‡] and Paul A. Lindahl*[,†,‡]

[†]Department of Biochemistry and Biophysics, Texas A&M University, College Station, Texas 77843-2128, United States

[‡]Department of Chemistry, Texas A&M University, College Station, Texas 77843-3255, United States

Supporting Information

ABSTRACT: Vacuoles were isolated from fermenting yeast cells grown on minimal medium supplemented with 40 μM ^{57}Fe. Absolute concentrations of Fe, Cu, Zn, Mn, Ca, and P in isolated vacuoles were determined by ICP-MS. Mössbauer spectra of isolated vacuoles were dominated by two spectral features: a mononuclear magnetically isolated high-spin (HS) Fe^{III} species coordinated primarily by hard/ionic (mostly or exclusively oxygen) ligands and superparamagnetic Fe^{III} oxyhydroxo nanoparticles. EPR spectra of isolated vacuoles exhibited a $g_{ave} \sim 4.3$ signal typical of HS Fe^{III} with E/D ~ 1/3. Chemical reduction of the HS Fe^{III} species was possible, affording a Mössbauer quadrupole doublet with parameters consistent with O/N ligation. Vacuolar spectral features were present in whole fermenting yeast cells; however, quantitative comparisons indicated that Fe leaches out of vacuoles during isolation. The *in vivo* vacuolar Fe concentration was estimated to be ~1.2 mM while the Fe concentration of isolated vacuoles was ~220 μM. Mössbauer analysis of Fe^{III} polyphosphate exhibited properties similar to those of vacuolar Fe. At the vacuolar pH of 5, Fe^{III} polyphosphate was magnetically isolated, while at pH 7, it formed nanoparticles. This pH-dependent conversion was reversible. Fe^{III} polyphosphate could also be reduced to the Fe^{II} state, affording similar Mössbauer parameters to that of reduced vacuolar Fe. These results are insufficient to identify the exact coordination environment of the Fe^{III} species in vacuoles, but they suggest a complex closely related to Fe^{III} polyphosphate. A model for Fe trafficking into/out of yeast vacuoles is proposed.

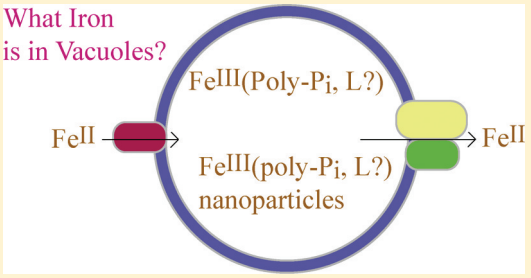

Yeast vacuoles are major hubs for iron trafficking and have many Fe-related functions.[1−3] One function is to *sequester* and *detoxify* Fe, so as to restrict the formation of reactive oxygen species that would otherwise be toxic to the cell.[2,4] Vacuoles also function as *reservoirs* of Fe, allowing cells to survive in Fe-deficient environments[2,5] and transition from fermenting to respiring metabolism.[6] They also *buffer* cytosolic Fe against fluctuations, so as to maintain cellular Fe homeostasis.[5]

Raguzzi et al.[6] and Singh et al.[3] have proposed that vacuoles contain ferric ions coordinated by hydroxide, phosphate, and/or polyphosphate ions. They suggested the Fe^{III} oxidation state because the vacuolar lumen is more acidic than the cytosol, which raises the effective electrochemical potential of the glutathione disulfide/glutathione couple. This couple dominates the redox status of the vacuole and cytosol; a higher effective potential translates into diminished reducing power. Phosphate and polyphosphate have been suggested as ligands because of the high concentration of these species in vacuolar lumen[3,7] and the ability of these anions to bind Fe^{III} ions tightly.[8,9]

Fe is imported into vacuoles through two major pathways, including endocytosis and through Ccc1p, a transporter on the vacuolar membrane.[10,11] The exact species imported is unknown, but the Fe^{II} state is generally assumed.[2,5,12] *CCC1* gene expression is responsive to cytosolic Fe concentrations and the *CCC1* mRNA is destabilized under Fe-deficient growth conditions.[13] Vacuoles isolated from cells that could not engage in endocytosis were phenotypically normal and contained proportionately more Fe/mg protein than found in Δ*ccc1* vacuoles.[2] These results suggest that the Ccc1p pathway is responsible for a larger portion of the Fe imported into the vacuole, relative to the endocytosis pathway.[14]

The vacuole membrane contains two Fe export systems: Fth1p/Fet5p[15] and Smf3p.[16] Fet5p and Fth1p are homologues of the plasma membrane multicopper oxidase Fet3p and permease Ftr1p.[3] These two plasma-membrane proteins form a complex that transports Fe^{III} from the environment into the cytosol, reducing it to the Fe^{II} state in the process. Fet5p and Fth1p are presumed to function similarly. Fre1p catalyzes the reduction of Fe^{III} to Fe^{II} by NADPH prior to delivering this ion to the Ftr1p/Fet3p complex.[17,18] Fre6p catalyzes the analogous reduction during the export of vacuolar Fe.[3,19] The vacuolar membrane protein Smf3p exports Fe (and other divalent metal ions) from the vacuolar lumen to the cytosol under low-Fe growth conditions.[16,20,21]

Received: September 24, 2011
Revised: October 24, 2011
Published: November 2, 2011

In summary, the import of Fe^{II} from the cytosol to the vacuole appears to be associated with its oxidation to Fe^{III}, and the export of Fe^{III} from the vacuole to the cytosol is associated with the reduction of Fe^{III} back to Fe^{II}. This scenario is reasonable and well-grounded from a biochemical/genetics perspective, but it has not been examined using biophysical methods. In the study described here, we isolated vacuoles from fermenting WT *S. cerevisiae* cells and characterized their Fe content using Mössbauer, EPR, and UV−vis spectroscopies as well as ICP-MS. We demonstrate that the Fe in this organelle consists predominately of mononuclear nonheme high-spin (HS) Fe^{III} ions, mostly likely as a single complex. A second species consisting of Fe^{III} oxyhydroxo nanoparticles is also present. The two species probably interconvert in a pH-dependent fashion.

EXPERIMENTAL PROCEDURES

Saccharomyces cerevisiae strain W303 (*MATα, ura3-1, ade2-1, trp1-1, his3-11,15, leu2-3,112*; ATCC) cells were maintained on YPAD (Yeast extract, peptone, adenine, glucose) plates. Starting from a single colony, cells were grown in liquid culture on minimal medium containing 2% w/v glucose and modified yeast nitrogen base (MP Bio) lacking copper and iron. Copper sulfate (10 μM final concentration) and ^{57}Fe citrate (40 μM final concentration) were added separately.

Isolation of Vacuoles. 1 L cell cultures (inoculated from 50 mL cultures) were grown to an OD (600 nm) ∼ 1 and then inoculated into 25 L cultures. The 25 L cultures were grown to an OD (600 nm) of 0.6−0.8 and harvested by centrifugation at 4000*g* for 5 min (Sorvall Evolution RC centrifuge, SLC-6000 rotor). The cell pellet was transferred to a refrigerated argon-atmosphere glovebox (MBraun Labmaster, 6 °C, ∼ 2 ppm of O_2) where vacuoles were isolated essentially as described,[3] except that cells were treated with ∼1000 U lyticase/g of wet cell paste for 50−90 min at 30 °C (Sigma-Aldrich). In some batches (Table S1), TCEP-HCl (tris(2-carboxyethyl)-phosphine, Thermo Scientific, #20491; 5 mM final concentration) was used instead of dithiothreitol (DTT, 10 mM final). Cells were disrupted using 100 μg/mL of diethylaminoethyl dextran (DEAE-Dextran, Sigma-Aldrich) in 15% Ficoll (Fisher Bioreagents) buffer.[22] The resulting cell lysate was subjected to density gradient centrifugation (Beckman Coulter Optima L-90K ultracentrifuge, SW-32 Ti rotor; 110,000g, 90 min). The first gradient consisted of cell lysate in 15% Ficoll buffer and with a layer of PS buffer on top. Typical volumes for the three layers were 20, 8 and 5 mL, respectively, from bottom to top. The material collected from the PS−8% interface was diluted with 15% Ficoll buffer and overlaid with 4% Ficoll buffer and with a layer of PS buffer on top. Volumes for this gradient were the same as for the first gradient. Purified vacuoles were collected at the PS−4% interface. Vacuoles were washed in PS buffer and centrifuged at 38000*g* for 20 min. Pelleted organelles were resuspended in PS buffer and packed into into Delrin Mössbauer cups (12 mm o.d. × 10 mm) and Suprasil quartz EPR tubes (Wilmad Labglass; 4 mm o.d.; 89 mm long) were packed by centrifugation at 10900*g* for 45 min. Cups and tubes were frozen and stored in liquid N_2 for subsequent analysis. Mössbauer and EPR spectra were obtained as described.[23] EPR signals were integrated using a program written in Matlab. The $g = 4.3$ signal was integrated in the 1000−2500 G range using a 1 mM CuEDTA standard at 10 K and 0.2 mW. Baselines were corrected using a second-order polynomial fit through baseline regions on both sides of the signals. Double integral values obtained were multiplied by 3 to account for the total spin population of all three doublet levels of the $S = 5/2$ manifold. Spin concentrations were then calculated as described.[24] UV−vis spectra of vacuole suspensions in a 2 mm path length quartz cuvette were collected using a Hitachi Model U3310 spectrophotometer with a head-on photomultiplier tube.

Whole Cell Samples. Cells were grown to OD(600 nm) ∼ 1 and inoculated into 1 L cultures, as described above. 1 L cell cultures were grown to OD(600 nm) ∼ 1 and harvested by centrifugation at 4000*g* for 5 min (Beckman Coulter Avanti J-26 XP centrifuge, JS-5.3 rotor). Cells were washed with deionized H_2O, then with 100 μM unbuffered EDTA three times, and three times more with H_2O. Washed cells were packed by centrifugation into Mössbauer cups (12 mm o.d. × 10 mm) and Suprasil quartz EPR tubes at 4000*g* for 10 min.

Western Blot Analysis and Electron Microscopy. Protein concentrations were determined using the BCA method.[25] Western blots used 60 μg of vacuolar or cell extract protein per lane, and mitochondrial porin (Invitrogen), vacuolar carboxypeptidase Y (CPY) (AbCam), cytosolic 3-phosphoglycerate kinase (PGK) (Invitrogen), and endoplasmic reticular Kar2 (Santa Cruz Biotechnology) proteins were detected. Goat anti-mouse HRP-conjugated secondary antibodies (Invitrogen) were used with Porin and PGK, while goat anti-rabbit HRP-conjugated secondary antibodies (Santa Cruz Biotechnology) were used with CPY and Kar2. Enhanced chemiluminescent western blotting substrate (Thermo Scientific) was added, and images were obtained (FujiFilmLAS-4000 mini) with a 10 s standard exposure and the chemiluminescence setting. Images were analyzed using MultiGuage version 3.1.

For electron micrographs, samples were fixed in 1% acrolein (isolated vacuoles) or 5% acrolein (whole cells) (Sigma-Aldrich) solutions at 4 °C with shaking and then rinsed 4 times with 1% dimethyl sulfoxide (DMSO) and stored overnight at 4 °C. The alkaline phosphatase reaction was performed as described.[26,27] Samples were fixed overnight with 1% osmium tetroxide (OsO_4) and then dehydrated using a cold methanol series. Samples were infiltrated using three 100% changes of Quetol/Araldite/DDSA resin and polymerized. Ultrathin sections were cut using an Ultracut E microtome (Reichert-Jung), visualized using a transmission electron microscope (JEOL 1200-EX), and photographed using a bottom-mounted 3K × 3K, slow scan, lens-coupled CCD camera (SIA 15C).

Packing Efficiency of Isolated Vacuoles. The packing efficiency of vacuoles was determined as described.[28] Briefly, the fractional volume of interstitial buffer in packed vacuoles was calculated using the cell-impermeable fluorescent compound 5.[29] Vacuoles were isolated from cells grown to OD(600 nm) ∼ 0.8, transferred to an EPR tube, and pelleted by centrifugation (10900*g*, 45 min). The volume of the pellet (V_{pel}) was determined from its height in 3.0 mm i.d. EPR tubes. The pellet was resuspended using 200 μL of buffer containing 0.1 M compound **5**. The vacuoles were pelleted, the supernatant fraction was collected, and its volume determined (V_{sup1}). The concentration of compound **5** in the supernatant fraction (C_{sup1}) was determined from a standard curve generated using a fluorescence spectrometer (Koala 90080; ISS Inc.). Fluorescence was detected at 654 nm (fixed) with ten scans per sample. Pellet volumes were assumed to be due exclusively to vacuole and buffer volumes ($V_{pel} = V_{vacl} + V_{bufl}$). The conservation of matter requires that the molar amount of compound **5** added in the buffer

$$20\ \text{nmol} = C_{sup1}V_{sup1} + C_{sup1}V_{buf1}$$

Solving for V_{buf1} allowed the packing efficiency of vacuoles, defined as $(V_{pel} = V_{buf1})V_{pel} \times 100$, to be determined. The same steps were repeated with buffer lacking the compound. In this case

$$C_{sup1}V_{buf1} = C_{sup2}V_{sup2} + C_{sup2}V_{buf2}$$

The equation was solved for V_{buf2}, and packing efficiency was defined as $(V_{pel} = V_{buf2})V_{pel} \times 100$. V_{pel} was found to be unchanged with each centrifugation step.

Metal Concentrations. Pellets of isolated vacuoles (typically with volumes ranging from 50 to 100 μL) were resuspended in sufficient PS buffer for the suspension volume to total 225 μL. Suspensions were separated into aliquots of 50, 75, and 100 μL using 15 mL plastic screw-top vials. Concentrated (70%) trace-metal-grade (TMG) nitric acid (Fisher Chemicals) (100 μL) was added to each vial. Vials were sealed with screw-top caps wrapped tightly with electrical tape and then incubated at 90 °C for ~17 h. Aliquots were diluted to 7.9 mL using high-purity trace-metal-free double-distilled–deionized (DDDI) water generated using a Teflon sub-boiling still (Savillex). Samples were analyzed using ICP-MS (Agilent 7700x) utilizing both H_2 reaction mode (^{57}Fe and ^{56}Fe) and He collision modes (Mn, Cu, Zn, and P) to eliminate interferences. Standards were prepared from stock solutions (Inorganic Ventures), concentrated TMG nitric acid, and DDDI water. Calibration curves with a range of 0–1000 ppb were generated for each element as well as for the two isotopes of Fe.

Redox Activity of Fe in Isolated Vacuoles. After collecting the 7 K low-field Mössbauer spectrum of a preparation of isolated vacuoles (Table S1 and Figure S2B, batch 14), the sample was brought into the glovebox, thawed, and suspended in PS buffer containing 1% deoxycholate (final concentration). The suspension (200 μL) was transferred to a 2 mm path length quartz cuvette, which was sealed with a rubber septum and removed from the box. After collecting the UV–vis spectrum, the sample was returned to the box and treated with dithionite (400 μM, final concentration), and another UV–vis spectrum was collected after ca. 5 min incubation. The sample was returned to the box, transferred to a Mössbauer cup, and frozen in liquid N_2.

Preparation of Fe Complexes. Sodium phosphate (dihydrate, Sigma-Aldrich) (50 mM final) and aqueous $^{57}Fe^{III}$ (5 mM, final) were mixed in an acetate/acetic acid buffer (100 mM, pH ~ 5 final) in an effort to generate Fe^{III} phosphate. The same approach was used to prepare Fe^{III} polyphosphate, except that sodium polyphosphate (Thermo-Fisher) was used. The aqueous $^{57}Fe^{III}$ stock solution was prepared by dissolving ^{57}Fe metal (Isoflex USA) in concentrated TMG HNO_3 (Fisher Scientific) and concentrated TMG HCl (Thermo-Fisher Scientific) in a 1:1 ratio and then diluted with DDDI H_2O to a final ^{57}Fe concentration of 80 mM and a final acid content of ~0.5%. To ensure complete oxidation, samples were treated using an excess of H_2O_2 (Thermo-Fisher Scientific).

RESULTS

Bioanalytical Characterization of Isolated Vacuoles. We isolated vacuoles from 23 independent batches of WT yeast cells, each grown under fermenting conditions using minimal medium supplemented with 40 μM ^{57}Fe (or ^{56}Fe) citrate. Each batch could not be analyzed by every method available due to insufficient material; Table S1 lists which batches were analyzed by which methods. Purity and membrane integrity were evaluated by electron microscopy (Figure 1, top panel) and

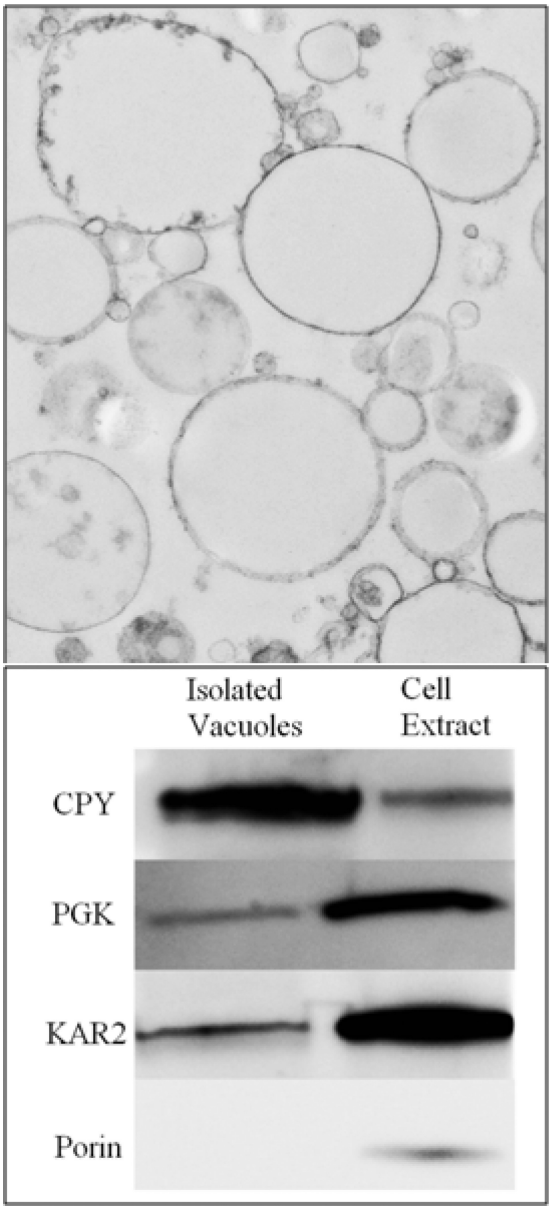

Figure 1. TEM images and Western Blots of isolated vacuoles. Top panel: images of batch 6 vacuoles obtained at 10 000× magnification. Bottom panel: isolated vacuoles from batch 2 (lane 1) were compared with cell extract (lane 2).

Western Blot analysis (Figure 1, bottom panel). Electron micrographs revealed a dominance of intact vacuolar membranes in the samples. Additional TEM images are provided in Figure S1. Relative to the cell-extract lane, isolated vacuoles contained 3-fold more CPY, a vacuolar marker protein, 5-fold less KAR2, an ER protein, 16-fold less of mitochondrial Porin, and 4-fold less of the cytosolic protein PGK. Overall, this analysis suggests that our isolated vacuoles were largely intact and purified, with minor contamination of ER, mitochondrial, and cytosolic proteins.

dx.doi.org/10.1021/bi2014954|*Biochemistry* 2011, 50, 10275–10283

We determined the packing efficiency of isolated vacuoles using a fluorescent compound that does not penetrate cellular plasma membranes.[29] Neither does this compound appear to penetrate vacuolar membranes, in that samples exposed to it and then washed repeatedly did not exhibit substantial fluorescence beyond that of unexposed samples. The percentage of the volume of packed vacuoles due to the vacuoles themselves, taken as the average of the six values (Table S2), was 76 ± 5%. The remainder was assumed to be due to interstitial buffer.

The concentrations of Fe, Cu, Zn, Mn, Ca, and P in 18 batches of isolated vacuoles (taking packing efficiency into account) were determined (Table S3); averages ± SD in μM were Fe, 220 ± 100; Cu (low) 30 ± 30; Cu (high) 540 ± 280; Zn, 160 ± 120; Mn, 1.7 ± 0.6; Ca, 190 ± 110; and P, 14 000 ± 8700. Batch-to-batch variability was significant, with relative errors of ca. ±60% or higher. This suggests that there are unknown and uncontrolled variables in our growth and/or isolation procedures. Cu concentrations were especially scattered, but they bifurcated rather cleanly into low and high groups. The low Cu concentrations are perhaps more reliable, in that they are more consistent with the concentration of Cu in whole cells (see below). Mn concentrations were the least scattered. Phosphorus levels, which almost certainly reflect phosphate and polyphosphate ions, were orders of magnitude higher than the metal ion concentrations. The $[Fe]_{ave}/[protein]_{ave}$ ratio of 1.9 μg Fe/mg protein was 10-fold higher than in previous reports,[2,3] suggesting that our vacuoles contained more Fe (or less protein, or some combination of the two) than those studied previously. For the 16 batches isolated from cells grown on media enriched in ^{57}Fe, the average level of enrichment was 74 ± 13%. The Fe concentration in a batch of whole WT cells grown on the same media was 380 μM, similar to the value of 440 μM previously reported.[28]

Spectroscopic Characterization of Isolated Vacuoles.

Figure 2 shows the variable field, variable temperature Mössbauer spectra of isolated vacuoles from batch 15. The 4.3 K, 0.05 T spectrum (Figure 2A) was dominated by a paramagnetic species with absorption between −10 and +10 mm/s. This spectral feature is typical of a mononuclear HS Fe^{III} species and was analyzed with a $S = 5/2$ spin-Hamiltonian

$$\mathcal{H} = D(S_z^2 - 35/12) + E(S_x^2 - S_y^2) + \beta S\cdot g\cdot B + S\cdot A\cdot I - g_n\beta_n\cdot B\cdot I + \mathcal{H}_Q$$

where D and E are the axial and rhombic zero-field-splitting parameters, A is the ^{57}Fe magnetic hyperfine tensor, and $\mathcal{H}_Q$ describes the nuclear quadrupole interactions.

This feature represented 75% of the overall spectral intensity in this batch. Residual intensity was unresolved and centered near 0 mm/s. At 7 K and 0.05 T (Figure 2B) the middle doublet ($m_s = \pm 3/2$) of the $S = 5/2$ spin multiplet had an appreciable population, shown by the strong absorption features in the +4 and −4 mm/s region. This indicated that D was small. Mössbauer and EPR fitting trials suggested that $D = 0.5$ cm^{-1} and $E/D = 0.33$ (rhombic symmetry). The fitted isomer shift, quadruple splitting, and isotropic hyperfine coupling constant (−230 kG) suggest a hexacoordinated HS Fe^{III} species.[30] The isotropic hyperfine coupling constant is near the limit of that observed for HS Fe^{III} systems with rhombic symmetry, and it indicates very hard/ionic donor atoms.[30] $A_0/g_N\cdot\beta_N$ values for $[Fe^{III}(H_2O)_6]^{3+}$,[31] ammonium iron alum $(NH_4Fe(SO_4)_2\cdot 12H_2O)$,[32] and HS Fe^{III} polyphosphate (see below) are within this limiting region (ca. −238 kG), suggesting that the vacuolar HS Fe^{III} species is coordinated by similar oxygen donors.

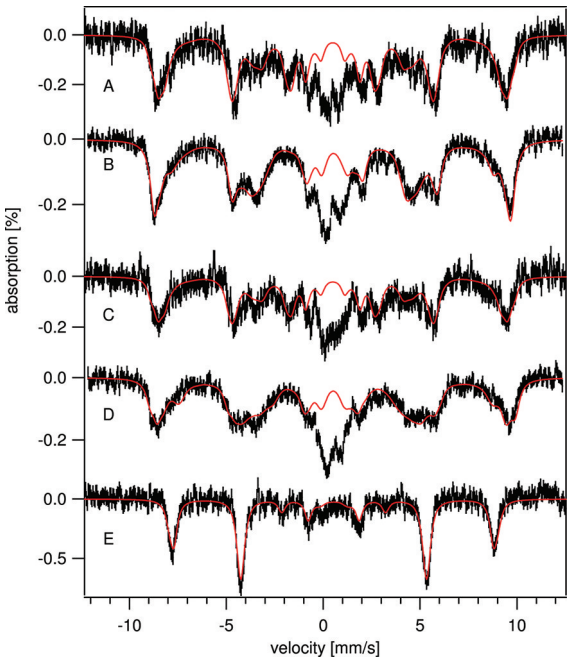

Figure 2. Mössbauer spectra of isolated vacuoles (batch 15): A, 4.2 K, 0.05 T; B, 7 K, 0.05T; C, 12 K, 0.05 T; D, 100 K, 0.05 T; E, 4.2 K, 6 T. Applied fields in (A, E) were perpendicular to the γ-radiation, while those in (B−D) were parallel to the radiation. The solid red lines are simulations assuming $S = 5/2$, $D = 0.5$ cm^{-1}, and $E/D = 0.33$, $A_0/g_N\cdot\beta_N = -230$ kG, $\delta = 0.54$ mm/s, $\Delta E_Q = 0.39$ mm/s, and $\eta = 2.8$.

The spectra of all batches examined by Mössbauer also included a second component in varying relative proportions. The batch just described (batch 15) exhibited the lowest proportion of this component, while batch 23 exhibited the highest proportion (Figure 3). The spectra of three other batches, with intermediate levels of the second component, are shown in Figure S2. In batches showing greater resolution of this second feature, a quadrupole doublet was evident. These parameters were similar to those of Fe^{III} (phosphorus) oxyhydroxo nanoparticles observed in various genetic strains of yeast.[23,28,33,34] The spectral features due to the nanoparticles could be removed, affording difference spectra (Figure 3C,F) that could be simulated using the same HS Fe^{III} parameters as used above. A somewhat different spectral shape was reported previously,[23,28,33,34] but in those spectra the field was applied *parallel* to the γ-radiation, affording different selection rules. The magnetic features due to these nanoparticles in Figure 3 were broad because the hyperfine coupling tensor A values were widely distributed as is typical of aggregated superparamagnetic materials.

X-band EPR spectra of isolated vacuoles supported this analysis, as all 10 batches examined displayed a dominant feature at $g_{ave} \sim 4.3$ (Figure 4A). Such features are typical of HS Fe^{III} species with rhombic symmetry ($E/D \sim 1/3$). However, the quantified intensity of the signal varied considerably, with spin concentrations ranging from 110 to 175 μM in samples of packed isolated vacuoles from four separate batches (batches 14, 16, 17, and 23). When normalized to the [Fe], and to the

dx.doi.org/10.1021/bi2014954|*Biochemistry* 2011, 50, 10275−10283

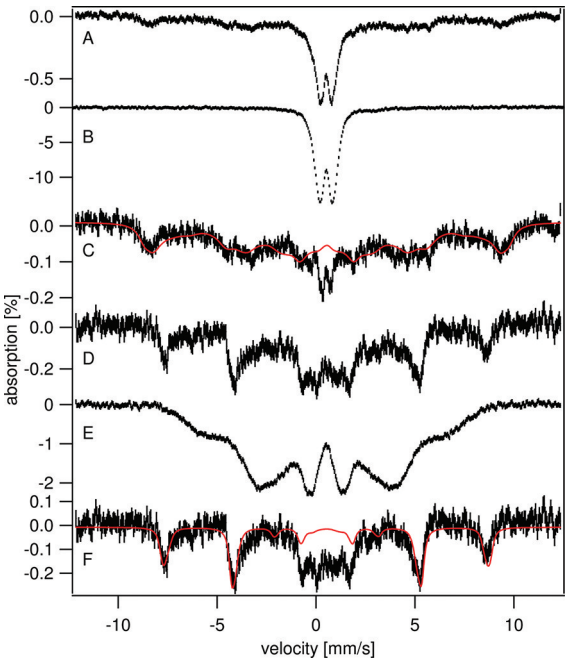

Figure 3. Mössbauer spectra of isolated vacuoles (batch 23) and mitochondria isolated from a genetic strain (Aft1-1^{up}) known to contain Fe^{III} (phosphate) nanoparticles:[28] A, vacuoles at 7 K and 0.05 T; B, mitochondria at 4.3 K and 0.05 T; C, same as A after spectrum B was subtracted at the 40% level. The solid red line is a simulation assuming the parameters specified in Figure 2. D, vacuoles at 4.2 K and 6 T; E, mitochondria at 4.2 K and 6 T. This sample was the same as in Figure 3A of reference 27. F, same as D after spectrum E was subtracted at the 40% level. The solid line is a simulation assuming the same parameters as in C, except that the applied field was 6 T. In D and E, applied fields were perpendicular to the γ-radiation. In A and B, applied fields were parallel to the radiation.

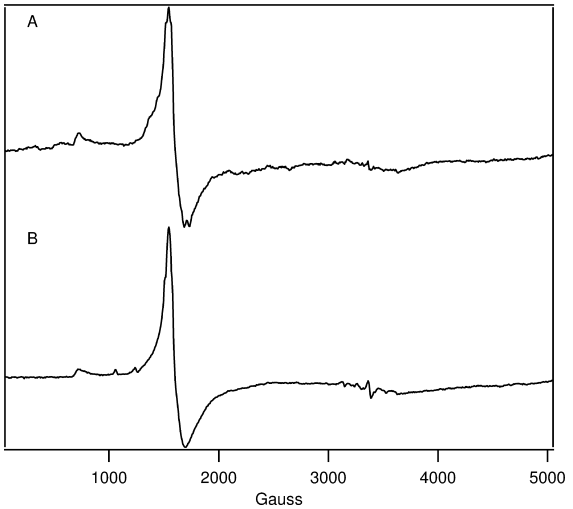

Figure 4. EPR of isolated vacuoles (A) and whole cells (B): A, batch 23; temperature, 4 K; microwave frequency, 9.46 GHz; microwave power 0.08 mW; B, temperature, 10 K; microwave frequency, 9.46 GHz; microwave power 0.2 mW. The whole-cell spectrum includes low-intensity features at g = 6.4 and 5.4 and signals in the g = 2 region which are absent or of diminished intensity in the spectrum of isolated vacuoles. These features originate from mitochondria.[23,46] The whole-cell spectrum includes low-intensity features at g = 6.4 and 5.4.[23,46] The low-field features probably arise from cytochrome c oxidase while the high-field features arise from other respiration-related proteins.

fraction of Fe associated with the six-line pattern in the Mössbauer spectra (measured to be 56% and 85% in batches 23 and 14, respectively, and assumed to be midway between these percentages in batches 17 and 16), the ratio of [spin]/[HS Fe^{III}] was 0.9, 0.7, 0.8, and 0.6, respectively.[a] No Cu^{II}-based EPR signals were observed, even in the four batches examined that had high Cu concentrations (batches 8, 20, 21, and 22). Cu ions in the organelle may be in the cuprous state, which is counterintuitive given the oxidizing environment of the vacuolar lumen. They may also be in the cupric state and EPR-silent for other reasons, e.g., involving spin-coupling.

When suspended in buffer, solutions of isolated vacuoles were milky white and have electronic absorption spectra dominated by the effects of light scattering (Figure 5, top

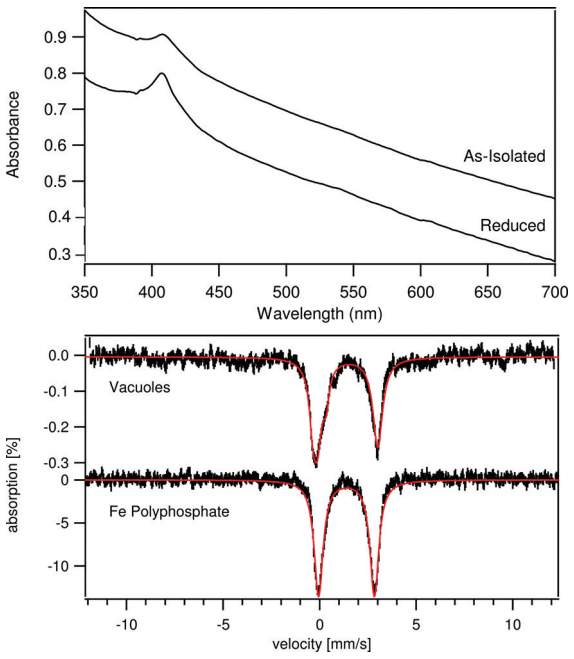

Figure 5. Electronic absorption spectra of isolated vacuoles (batch 15), before and after treatment with a reductant (upper panel), and Mössbauer spectrum of the same after treatment with a reductant (lower panel). The corresponding Mössbauer spectrum prior to adding the reductant is shown in Figure S2, spectrum B. The 6 K, 0.05 T Mössbauer spectrum of Fe^{III} polyphosphate (pH 7) after treatment with dithionite is also shown in the lower panel. The red lines are simulations assuming (vacuoles) δ = 1.41 mm/s and ΔE_Q = 3.15 mm/s and (^{57}Fe^{III} polyphosphate) δ = 1.39 mm/s and ΔE_Q = 2.88 mm/s.

panel). We considered that the low-intensity feature at ~410 nm was due to the HS Fe^{III} species evidenced by Mössbauer and EPR spectra, as it reminded us of the broad low-intensity transition at 470 nm from diferric transferrin.[35] However, subsequent treatment with dithionite had no effect on this feature (Figure 5, top panel). The effectiveness of dithionite in reducing the HS Fe^{III} species was evidenced by the quadrupole doublet generated in the Mössbauer spectrum of the treated sample (Figure 5, bottom panel). We conclude that the dominant HS Fe^{III} species in as-isolated vacuoles is redox-active and can be reduced to the Fe^{II} state. However, neither redox state is associated with the observable electronic absorption feature. The Mössbauer parameters associated with the Fe^{II} doublet suggest that this species is primarily coordinated by oxygen and/or nitrogen donor ligands. Whether the exchange

of one ligand set for another accompanies reduction remains undetermined.

Related Fe^{III} Compounds. We attempted to reproduce the mononuclear HS Fe^{III} species in vacuoles by adding phosphate and polyphosphate ions to hex(aqua/hydroxo) Fe^{III} ions in pH 5 buffer. This pH was used to mimic the vacuolar lumen, which has pH between 4.8 and 5.4.[36] Presuming that the intended complexes formed, the 6 K and 0.05 T Mössbauer spectrum of Fe^{III} phosphate (Figure 6A) and Fe^{III} hex(aqua/hydroxo) species (data not shown) exhibited features typical of Fe^{III} oxyhydroxo nanoparticles. In contrast, the spectrum of Fe^{III} polyphosphate (Figure 6B) exhibited features associated with mononuclear HS Fe^{III} ions with similar parameters to those used to fit the equivalent spectrum in Figure 2B. After data collection, the Fe^{III} polyphosphate sample was thawed, adjusted to pH = 7, and refrozen. The resulting Mössbauer spectrum (Figure 6C) indicated the presence of both nanoparticles and HS Fe^{III} ions. This suggests that mononuclear HS Fe^{III} polyphosphate can convert to Fe^{III} nanoparticles simply by raising the pH. The nanoparticle-forming reaction was reversible, in that thawing the pH 7-adjusted sample, lowering its pH to 4, and refreezing it resulted in a Mössbauer spectrum, again indicating the mononuclear HS Fe^{III} state. In contrast, the Fe^{III} (phosphate) nanoparticles at pH 5 could not be converted into the mononuclear HS Fe^{III} state by lowering the pH to 3, 2, and finally 1. Similar to the Fe species in vacuoles, the Fe^{III} polyphosphate sample could be reduced by dithionite, resulting in a quadrupole doublet (Figure 5, bottom panel) with parameters very similar to that observed when the HS Fe^{III} complex in vacuoles was reduced.

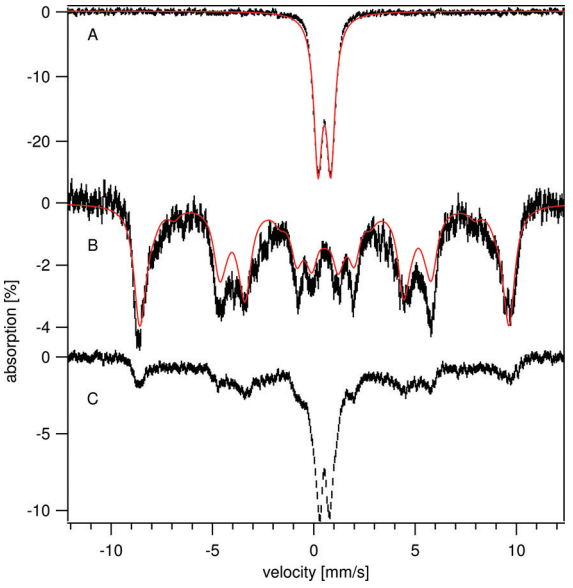

Figure 6. 6 K and 0.05 T Mössbauer spectra of $^{57}Fe^{III}$ phosphate (A) and $^{57}Fe^{III}$ polyphosphate (B, C) at different pH values: A, $^{57}Fe^{III}$ phosphate at pH 5; B, $^{57}Fe^{III}$ polyphosphate at pH 5; C, $^{57}Fe^{III}$ polyphosphate at pH 7. Applied fields were parallel to the γ-radiation. Samples were prepared in 0.1 M acetate/acetic acid buffer (pH 5), and excess H_2O_2 was added to each sample to obtain an oxidizing environment. The solid line in part A is a simulation assuming $\delta = 0.53$ mm/s and $\Delta E_Q = 0.63$ mm/s. The solid line in part B is a simulation assuming $S = 5/2$, $D = 0.5$ cm^{-1}, $E/D = 0.33$, $A_0/g_N \cdot \beta_N = -238$ kG, $\delta = 0.54$ mm/s, $\Delta E_Q = 0.39$ mm/s, and $\eta = 3$.

Whole Cells. We calculated the concentration of Fe (and other metal ions) within fermenting yeast cells grown in the same medium used to grow the cells from which vacuoles were isolated. Measured values using packed cells were normalized using the previously determined packing efficiency.[37] Low-temperature Mössbauer spectra of whole cells (Figure 7) were dominated by the same pattern that was observed in spectra of isolated vacuoles, i.e., typical of a mononuclear HS Fe^{III} species. EPR spectra of same whole cells from which the vacuoles of Figure 4A were isolated were dominated by a $g_{ave} = 4.3$ signal (Figure 4B), essentially indistinguishable from that of isolated vacuoles.

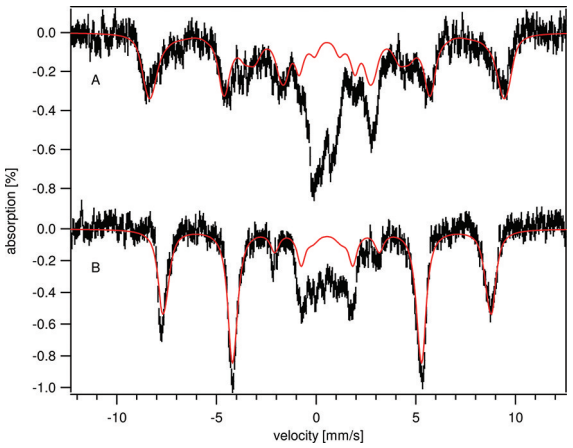

Figure 7. Mössbauer spectra of WT whole cells: A, 4.2 K and 0.05 T; B, 4.2 K and 6 T. Applied fields were perpendicular to the γ-radiation. The solid red lines are simulations assuming the parameters specified in Figure 2.

DISCUSSION

Two Types of Fe in Vacuoles. Our results indicate that vacuoles isolated from Fe-sufficient fermenting yeast cells contain two major types of Fe species. One is a mononuclear, magnetically isolated (i.e., soluble) HS Fe^{III} complex; the other is magnetically interacting (i.e., insoluble) Fe^{III} oxyhydroxo nanoparticles. The nanoparticles contained in Yah1p-depleted, Atm1p-depeleted, Yfh1p-depleted, and Aft1-1^{up} mitochondria have similar Mössbauer properties, and in the three cases investigated, phosphorus, presumed at the time to be in the form of phosphate ions, was found to be associated with this material.[23,28,33,34]

The composition and structure(s) of the Fe^{III} nanoparticles in vacuoles are unknown, including whether phosphate or a phosphate-related species is associated. We suspect that these nanoparticles are related to ferrihydrite, a metastable iron oxyhydroxo generated by titrating $Fe^{III}(NO_3)_3$ with hydroxide ions to pH ~ 7.5.[38] Ferrihydrite contains both octahedrally and tetrahedrally coordinated Fe^{III} ions.[39] When present, phosphate ions and other oxyanions coprecipitate with Fe^{III}.[40−42] This alters the structure, crystallinity, and superparamagnetic properties of the resulting nanoparticles.[43−45]

We propose that the two major forms of Fe in vacuoles interconvert by reactions promoted by a simple change in pH. As illustrated by the model in Figure 8, low pH (protonation) favors the mononuclear species while high pH (deprotonation) favors nanoparticles. Deprotonation of a ligand (e.g., water, phosphate, or polyphosphate group) on one isolated HS Fe^{III}

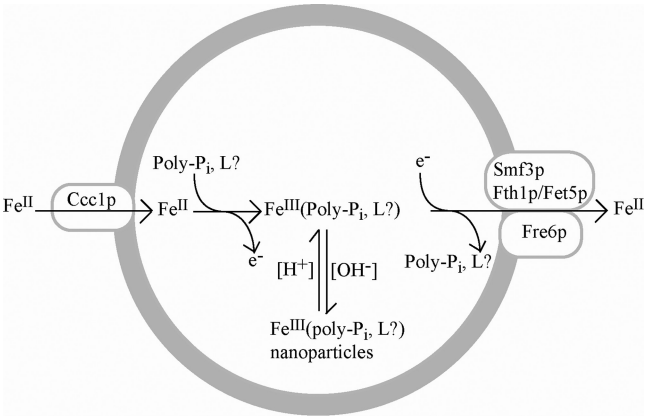

Figure 8. Model showing the dynamics of Fe import and export in yeast vacuoles. An unknown ferrous species enters the vacuole via Ccc1p. Associated with this import is the exchange of ligands and oxidation to HS Fe^{III}. Polyphosphate is suggested as a possible coordinated ligand, but further studies are required to establish this. Upon export, the HS Fe^{III} species is reduced to Fe^{II} and ligands are again exchanged. At pH > ca. 5, some or all of the species precipitates in the form or Fe^{III} (phosphate-based) oxyhydroxo nanoparticles perhaps associated with polyphosphate.

molecular species and dissociation of a ligand on a neighboring species (to create an open coordinate site) might be sufficient to promote an association between the two, ultimately generating nanoparticles. At the normal pH of vacuoles (pH ~ 5) we would expect that the majority of the Fe would be present as the mononuclear HS Fe^{III} species, as is observed in whole cells and in most batches of isolated vacuoles. Nanoparticles probably form when the pH of the vacuole lumen is somewhat higher than 5. Perhaps the pH of the vacuoles increases slightly during isolation, or the ratio of phosphate:polyphosphate in the vacuoles is altered. Studies are currently underway to test these hypotheses.

Our results are insufficient to identify the coordination environment of the HS Fe^{III} species unambiguously, but they are consistent with an Fe^{III} polyphosphate complex and inconsistent with an Fe^{III} phosphate complex or with hex(aqua/hydroxo) Fe^{III}. Of these three possibilities, only the Fe^{III} polyphosphate complex was present as a HS mononuclear species at the pH of the vacuolar lumen (pH ~ 5); the Fe^{III} phosphate and hex(aqua/hydroxo) complexes were present as nanoparticles. Fe^{III} phosphate remained as nanoparticles at pH's as low as 1 (the behavior of the hex(aqua/hydroxo) complex was not evaluated at lower pHs). Our results indicate that the HS Fe^{III} complex in vacuoles is closely related to an Fe^{III} polyphosphate complex, consistent with earlier and quite perceptive proposals by Lesuisse, Crichton, and Kosman that vacuolar Fe is bound by polyphosphate.[3,6] However, further studies are required to unambiguously identify the HS Fe^{III} complex in vacuoles.

Vacuolar Metal Concentrations. We report here the first absolute (micromolar) concentrations of the metal content of vacuoles; previously only *ratios* of metal concentrations divided by protein concentrations (or dry weight) had been reported. Such ratios cannot be used in mass-balance equations and are difficult to interpret because differences might arise from changes in either protein concentration or metal concentration (or some combination of the two). For example, in the current study, metal-to-protein ratios were found to be ~10-fold higher than previously reported.[2,3] Whether this is due to higher Fe concentrations or lower protein concentrations (or both) in our vacuoles cannot be determined.

We suspect that we achieved higher concentrations of Fe in isolated vacuoles than have been obtained previously due to our use of TCEP instead of DTT to prepare the cell wall for digestion by lyticase. Raguzzi et al.[6] reported that adding a chelator and reductant mobilizes vacuolar Fe stores, and DTT is a membrane-permeable reducing agent. TCEP is a membrane-impermeable reducing agent. EGTA was also excluded from our isolation buffers to avoid loss of vacuolar Fe, whereas EGTA is commonly added to buffer solutions to remove loosely bound Fe from membranes.

Loss of Fe from Vacuoles during Isolation. Vacuoles isolated from cells grown under fermenting conditions and in the presence of 40 μM Fe contained an average of ~220 μM Fe, with 56−85% present as a HS Fe^{III} species. Whole cells grown under the same conditions contained 380 μM Fe with ~75% of the Mössbauer spectral intensity due to what appears to be the same HS Fe^{III} species. Assuming that it is the same species and that it is located exclusively in vacuoles (which occupy ~25% of cell volume), the concentration of this species in vacuoles in whole cells is calculated to be ca. 1.2 mM. This is ca. 5 times higher than found in our isolated vacuole preps, implying that the majority of Fe in the vacuole is lost during isolation. Other groups have suggested that Fe leaches from vacuoles during isolation.[2] Given their function in the cell (dynamic storage and release of Fe as needed), it is not surprising that Fe can be easily mobilized from this organelle.

The export of Fe has been associated with its reduction.[3] Our results show that there is no buildup of HS Fe^{II} in the vacuole even though the Fe^{III} contained in the organelle is redox active (reducible by dithionite). We have not observed by Mössbauer spectroscopy any Fe^{II} in isolated vacuoles, suggesting that reduction of Fe^{III} to Fe^{II} is slower than the export of Fe^{II} from the vacuoles. Essentially, the Fe^{III} species is *trapped* in vacuoles, escaping immediately once it is reduced.

In the future, we plan to identify the mononuclear HS Fe^{III} species present in vacuoles. We also hope to use our biophysical methods, in conjunction with genetic and biochemical investigations, to explore the mechanisms of vacuolar Fe import and export and the regulation of these processes. Since vacuoles are a major hub of iron trafficking, understanding how they store and release iron is a prerequisite to better understanding cellular Fe metabolism.

■ ASSOCIATED CONTENT

Ⓢ Supporting Information

A summary of the batches prepared and characterized (Table S1), packing efficiency data (Table S2), elemental analysis and protein concentration analysis of isolated vacuoles and whole cells (Table S3), additional TEM images of isolated vacuoles (Figure S1), additional Mössbauer spectra of isolated vacuoles (Figure S2), and additional EPR spectra of isolated vacuoles (Figure S3). This material is available free of charge via the Internet at http://pubs.acs.org.

■ AUTHOR INFORMATION

Corresponding Author

*Phone: 979-845-0956. Fax: 979-845-4719. E-mail: Lindahl@chem.tamu.edu.

Funding

This study was supported by the National Institutes of Health (GM084266) and the Robert A. Welch Foundation (A1170).

■ ACKNOWLEDGMENTS

We thank E. Ann Ellis (Microscopy center, TAMU) for assistance in obtaining EM images, Marco Vilela (currently at Harvard University) for writing the Matlab code for the spin quantification, Kevin Burgess (Department of Chemistry, TAMU) for providing fluorescent compound **5**, and Ryland Young (Department of Biochemistry and Biophysics, TAMU) for use of his fluorescence spectrometer.

■ ABBREVIATIONS

WT, wild type; TCEP-HCl, tris(2-carboxyethyl)phosphine; DTT, dithiothreitol; DEAE, diethylaminoethyl; CPY, carboxypeptidase Y; PGK, phosphoglycerate kinase; DDSA, dodecenyl succinic anhydride; PIPES, piperazine-*N*,*N*′-bis(2-ethanesulfonic acid); PS buffer, buffer containing 20 mM PIPES and 0.2 M sorbitol, pH 6.8; DDDI, double-distilled and deionized; TMG, trace metal grade; TEM, transmission electron microscopy; δ, isomer shift; ΔE_Q, quadrupole splitting; HS, high spin; LS, low spin; EPR, electron paramagnetic resonance; ICP-MS, inductively coupled plasma mass spectrometry.

■ ADDITIONAL NOTE

[a]The temperature was unstable in the three determinations that afforded the lower values, due to a damaged quartz insert in the spectrometer. The experiment that yielded the value nearest to unity was obtained after a new insert was installed. With the new insert, temperatures at the sample were noticeably more stable. Thus, we believe that the 0.9 [spin]/[HS Fe^{III}] value is the most accurate of the four determinations.

■ REFERENCES

(1) Li, S. C., and Kane, P. M. (2009) The yeast lysosome-like vacuole: Endpoint and crossroads. *Biochim. Biophys. Acta, Mol. Cell Res. 1793*, 650−663.

(2) Li, L. T., Chen, O. S., Ward, D. M., and Kaplan, J. (2001) A yeast vacuolar membrane transporter CCC1 facilitates iron storage. *Mol. Biol. Cell 12*, 206a−206a.

(3) Singh, A., Kaur, N., and Kosman, D. J. (2007) The metalloreductase Fre6p in Fe-Efflux from the yeast vacuole. *J. Biol. Chem. 282*, 28619−28626.

(4) Corson, L. B., Folmer, J., Strain, J. J., Culotta, V. C., and Cleveland, D. W. (1999) Oxidative stress and iron are implicated in fragmenting vacuoles of *Saccharomyces cerevisiae* lacking Cu,Zn-superoxide dismutase. *J. Biol. Chem. 274*, 27590−27596.

(5) Kaplan, C. D., and Kaplan, J. (2009) Iron Acquisition and Transcriptional Regulation. *Chem. Rev. 109*, 4536−4552.

(6) Raguzzi, F., Lesuisse, E., and Crichton, R. R. (1988) Iron Storage in *Saccharomyces cerevisiae*. *FEBS Lett. 231*, 253−258.

(7) Paz, Y., Shimoni, E., Weiss, M., and Pick, U. (2007) Effects of iron deficiency on iron binding and internalization into acidic vacuoles in *Dunaliella salina*. *Plant Physiol. 144*, 1407−1415.

(8) Pan, B. J., Wu, J., Lv, L., Zhang, W. M., Xiao, L. L., Wang, X. S., Tao, X. C., Zheng, S. R., and Pan, B. C. (2009) Development of polymer-based nanosized hydrated ferric oxides (HFOs) for enhanced phosphate removal from waste effluents. *Water Res. 43*, 4421−4429.

(9) Rachmilovich-Calis, S., Masarwa, A., Meyerstein, N., and Meyerstein, D. (2011) The effect of pyrophosphate, tripolyphosphate and ATP on the rate of the Fenton reaction. *J. Inorg. Biochem. 105*, 669−674.

(10) Fu, D. D., Beeler, T., and Dunn, T. (1994) Sequence, Mapping and Disruption of Ccc1, a Gene That Cross-Complements the Ca2+-Sensitive Phenotype of Csg1Mutants. *Yeast 10*, 515−521.

(11) Lapinskas, P. J., Lin, S. J., and Culotta, V. C. (1996) The role of the *Saccharomyces cerevisiae* CCC1 gene in the homeostasis of manganese ions. *Mol. Microbiol. 21*, 519−528.

(12) Lin, H. L., Burton, D., Li, L. T., Warner, D. E., Phillips, J. D., Ward, D. M., and Kaplan, J. (2009) Gain-of-function mutations identify amino acids within transmembrane domains of the yeast vacuolar transporter Zrc1 that determine metal specificity. *Biochem. J. 422*, 273−283.

(13) Kumanovics, A., Chen, O. S., Li, L. T., Bagley, D., Adkins, E. M., Lin, H. L., Dingra, N. N., Outten, C. E., Keller, G., Winge, D., Ward, D. M., and Kaplan, J. (2008) Identification of FRA1 and FRA2 as genes involved in regulating the yeast iron regulon in response to decreased mitochondrial iron-sulfur cluster synthesis. *J. Biol. Chem. 283*, 10276−10286.

(14) Li, L. T., Chen, O. S., Ward, D. M., and Kaplan, J. (2001) CCC1 is a transporter that mediates vacuolar iron storage in yeast. *J. Biol. Chem. 276*, 29515−29519.

(15) Urbanowski, J. L., and Piper, R. C. (1999) The iron transporter fth1p forms a complex with the Fet5 iron oxidase and resides on the vacuolar membrane. *J. Biol. Chem. 274*, 38061−38070.

(16) Portnoy, M. E., Liu, X. F., and Culotta, V. C. (2000) *Saccharomyces cerevisiae* expresses three functionally distinct homologues of the Nramp family of metal transporters. *Mol. Cell. Biol. 20*, 7893−7902.

(17) Askwith, C., Eide, D., Van Ho, A., Bernard, P. S., Li, L., Davis-Kaplan, S., Sipe, D. M., and Kaplan, J. (1994) The FET3 gene of *S. cerevisiae* encodes a multicopper oxidase required for ferrous iron uptake. *Cell 76*, 403−410.

(18) Stearman, R., Yuan, D. S., Yamaguchi-Iwai, Y., Klausner, R. D., and Dancis, A. (1996) A permease-oxidase complex involved in high-affinity iron uptake in yeast. *Science 271*, 1552−1557.

(19) Rees, E. M., and Thiele, D. J. (2007) Identification of a vacuole-associated metalloreductase and its role in Ctr2-mediated intracellular copper mobilization. *J. Biol. Chem. 282*, 21629−21638.

(20) Cohen, A., Nelson, H., and Nelson, N. (2000) The family of SMF metal ion transporters in yeast cells. *J. Biol. Chem. 275*, 33388−33394.

(21) Nelson, N. (1999) Metal ion transporters and homeostasis. *EMBO J. 18*, 4361−4371.

(22) Dürr, M., Boller, T., and Wiemken, A. (1975) Polybase Induced Lysis of Yeast Spheroplasts - New Gentle Method for Preparation of Vacuoles. *Arch. Microbiol. 105*, 319−327.

(23) Lindahl, P. A., Morales, J. G., Miao, R., and Holmes-Hampton, G. (2009) Isolation of *Saccharomyces cerevisiae* Mitochondria for Mössbauer, EPR, and Electronic Absorption Spectroscopic Analyses. *Methods Enzymol. 456*, 267−285.

(24) Orme-Johnson, N. R., and Orme-Johnson, W. H. (1978) Detection and quantitation of free cytochrome P-450 and cytochrome P-450 complexes by EPR spectroscopy. *Methods Enzymol. 52*, 252−257.

(25) Smith, P. K., Krohn, R. I., Hermanson, G. T., Mallia, A. K., Gartner, F. H., Provenzano, M. D., Fujimoto, E. K., Goeke, N. M., Olson, B. J., and Klenk, D. C. (1985) Measurement of Protein Using Bicinchoninic Acid. *Anal. Biochem. 150*, 76−85.

(26) Kobayashi, T., Seguchi, H., and Robinson, J. M. (1991) Localization of Alkaline-Phosphatase Activity in Human Neutrophils. *J. Electron Microsc. 40*, 208−208.

(27) Robinson, J. M. (1985) Improved Localization of Intracellular Sites of Phosphatases Using Cerium and Cell Permeabilization. *J. Histochem. Cytochem. 33*, 749−754.

(28) Miao, R., Holmes-Hampton, G. P., and Lindahl, P. A. (2011) Biophysical Investigation of the Iron in Aft1−1(up) and Gal-YAH1 *Saccharomyces cerevisiae*. *Biochemistry 50*, 2660−2671.

(29) Jose, J., Loudet, A., Ueno, Y., Barhoumi, R., Burghardt, R. C., and Burgess, K. (2010) Intracellular imaging of organelles with new

water-soluble benzophenoxazine dyes. *Org. Biomol. Chem. 8*, 2052−2059.
(30) Que, L. (2000) *Physical Methods in Bioinorganic Chemistry: Spectroscopy and Magnetism*, University Science Books, Sausalito, CA.
(31) Sinnecker, S., Slep, L. D., Bill, E., and Neese, F. (2005) Performance of nonrelativistic and quasi-relativistic hybrid DFT for the prediction of electric and magnetic hyperfine parameters in ^{57}Fe Mössbauer spectra. *Inorg. Chem. 44*, 2245−2254.
(32) Greenwood, N. N., and Gibb, T. C. (1971) High-spin Iron Complexes, in *Mössbauer Spectroscopy*, pp 112−159, Chapman and Hall, London.
(33) Miao, R., Martinho, M., Morales, J. G., Kim, H., Ellis, E. A., Lill, R., Hendrich, M. P., Münck, E., and Lindahl, P. A. (2008) EPR and Mössbauer spectroscopy of intact mitochondria isolated from Yah1p-depleted *Saccharomyces cerevisiae*. *Biochemistry 47*, 9888−9899.
(34) Lesuisse, E., Santos, R., Matzanke, B. F., Knight, S. A., Camadro, J. M., and Dancis, A. (2003) Iron use for haeme synthesis is under control of the yeast frataxin homologue (Yfh1). *Hum. Mol. Genet. 12*, 879−889.
(35) Nowalk, A. J., Tencza, S. B., and Mietzner, T. A. (1994) Coordination of Iron by the Ferric Iron-Binding Protein of Pathogenic Neisseria Is Homologous to the Transferrins. *Biochemistry 33*, 12769−12775.
(36) Brett, C. L., Kallay, L., Hua, Z. L., Green, R., Chyou, A., Zhang, Y. Q., Graham, T. R., Donowitz, M., and Rao, R. (2011) Genome-Wide Analysis Reveals the Vacuolar pH-Stat of *Saccharomyces cerevisiae*. *PLoS One*, 6.
(37) Holmes-Hampton, G. P., Miao, R., Morales, J. G., Guo, Y. S., Münck, E., and Lindahl, P. A. (2010) A Nonheme High-Spin Ferrous Pool in Mitochondria Isolated from Fermenting *Saccharomyces cerevisiae*. *Biochemistry 49*, 4227−4234.
(38) Debnath, S., Hausner, D. B., Strongin, D. R., and Kubicki, J. (2010) Reductive dissolution of ferrihydrite by ascorbic acid and the inhibiting effect of phospholipid. *J. Colloid Interface Sci. 341*, 215−223.
(39) Michel, F. M., Ehm, L., Antao, S. M., Lee, P. L., Chupas, P. J., Liu, G., Strongin, D. R., Schoonen, M. A. A., Phillips, B. L., and Parise, J. B. (2007) The structure of ferrihydrite, a nanocrystalline material. *Science 316*, 1726−1729.
(40) Arai, Y., and Sparks, D. L. (2001) ATR-FTIR spectroscopic investigation on phosphate adsorption mechanisms at the ferrihydrite-water interface. *J. Colloid Interface Sci. 241*, 317−326.
(41) Khare, N., Martin, J. D., and Hesterberg, D. (2007) Phosphate bonding configuration on ferrihydrite based on molecular orbital calculations and XANES fingerprinting. *Geochim. Cosmochim. Acta 71*, 4405−4415.
(42) Rhoton, F. E., and Bigham, J. M. (2005) Phosphate adsorption by ferrihydrite-amended soils. *J. Environ. Qual. 34*, 890−896.
(43) Thibault, P. J., Evans, R. J., Dutrizac, J. E., and Rancourt, D. G. (2009) Mineralogical confirmation of a near-P:Fe=1:2 limiting stoichiometric ratio in colloidal P-bearing ferrihydrite-like hydrous ferric oxide. *Geochim. Cosmochim. Acta 73*, 364−376.
(44) Rancourt, D. G., Thibault, P. J., Evans, R. J., and Dutrizac, J. E. (2009) Mineralogical confirmation of a near-P:Fe=1:2 limiting stoichiometric ratio in colloidal P-bearing ferrihydrite-like hydrous ferric oxide. *Geochim. Cosmochim. Acta 73*, 364−376.
(45) Larese-Casanova, P., Haderlein, S. B., and Kappler, A. (2010) Biomineralization of lepidocrocite and goethite by nitrate-reducing Fe(II)-oxidizing bacteria: Effect of pH, bicarbonate, phosphate, and humic acids. *Geochim. Cosmochim. Acta 74*, 3721−3734.
(46) Hudder, B. N., Morales, J. G., Stubna, A., Münck, E., Hendrich, M. P., and Lindahl, P. A. (2007) Electron paramagnetic resonance and Mössbauer spectroscopy of intact mitochondria from respiring *Saccharomyces cerevisiae*. *J. Biol. Inorg. Chem. 12*, 1029−1053.